Erosive and Strand Burning of Stick Propellants, Part II: Theoretical Modeling of Erosive-Burning Processes

W. H. Hsieh* and K. K. Kuo†
The Pennsylvania State University, University Park, Pennsylvania 16802

Interior ballistic performance of unslotted single-perforated stick propellants in a large-caliber gun could be influenced significantly by erosive burning. To analyze erosive-burning phenomena, a comprehensive model, with special emphasis on the interaction of turbulence and combustion, was formulated to simulate erosive-burning processes occurring inside the center perforation of an unslotted NOSOL-363 stick propellant. The numerical results obtained from solving the theoretical model were validated by experimental data in terms of time variations of internal diameter distributions along the propellant grain. It was found that the erosive-burning phenomenon was caused by the enhanced heat feedback from the gas phase to the solid phase resulting from the combined effect of increased turbulence kinetic energy and turbulent heat-transfer rate.

Nomenclature

A_i = preexponential factor for reaction involving ith species, m³/kmole-s
a = flux model absorption coefficients, m^{-1}
b = covolume used in the Noble-Abel equation of state, m³/kg
$C_1,\ldots,C_4$ = turbulence constants for k and ϵ equations
C_p = constant pressure specific heat, J/kg-K
C_{R_1},C_{R_2} = turbulence constants for transport equation of reactedness
C_s = specific heat of stick propellant, J/kg-K
C_μ = turbulence constants for eddy viscosity
$DR1$ = group of species, having delayed reactions, pyrolyzed from propellant surface
$DR2$ = delayed reaction species generated from O and F species
E_a = activation energy, J/kmole
E_b = blackbody emissive power, $=\sigma T^4$, J/m²-s
F = fuel-rich species pyrolyzed from propellant
H = stagnation enthalpy of ith species, $\equiv \sum Y_j h_j + u_i u_i/2$, J/kg
I_r = outward radiation flux in positive radial direction, W/m²
J_r = inward radiation flux in negative radial direction, W/m²
k = turbulence kinetic energy, m²/s²
O = oxidizer species pyrolyzed from propellant surface
P = final product species
Pr = Prandtl number
p = pressures, N/m²
$Q_{s,\mathrm{ref}}$ = surface heat release due to pyrolysis at reference temperature, J/kg
$\dot{q}''_{\mathrm{rad}}$ = radiative heat flux absorbed by solid propellant surface, W/m²
R = gas constant, J/kg-K
R_A,R_B = reactednesses defined in Eqs. (3a) and (3b)
R_u = universal gas constant, J/kmole-K
$\Re$ = reflectivity
r = radial coordinate, m
r_b = propellant burning rate, m/s
r_i = inner radius of perforation, m
r_o = outer radius of stick propellant, m
Sc = Schmidt number
s = flux-modeling scattering coefficient, 1/m
T = temperature, K
t = time, s
u = gas velocity in axial direction, m/s
u_* = friction velocity, $=\sqrt{\tau_w/\rho}$, m/s
v = gas velocity in radial direction, m/s
W_i = molecular weight of ith species, kg/kmole
x = axial coordinate, m
y = distance away from wall, m
Y_i = mass fraction of ith species; i could represent F, O, $DR1$, $DR2$, or P
γ = specific-heat ratio
δ = boundary-layer thickness, m
ϵ = turbulence dissipation rate, m²/s³
ϵ_s = surface emissivity of solid propellant
λ = thermal conductivity, W/m-K
τ = shear stress, N/m²
μ = dynamic viscosity of gas, N-s/m²
μ_t = turbulent viscosity, N-s/m²
ν_i = number of kmole of ith species
ρ = density, kg/m³
σ = Stefan-Boltzmann constant, W/m²-K⁴
$\dot{\omega}_R$ = chemical production term defined in Eqs. (12a) and (12b), kg/m³-s

Subscripts

b = burned state
$\mathfrak{L}$ = centerline value
eff = effective
g = gas phase
i = internal perforation region
p = propellant
s = surface
u = unburned state
w = wall

Diacriticals

$\tilde{}$ = mass-weighted average quantity (Favre averaging)
$\bar{}$ = time-averaged quantity

Superscript

$''$ = fluctuation quantity in Favre averaging

Received July 8, 1988; revision received May 12, 1989.

*Assistant Professor, Department of Mechanical Engineering.
†Distinguished Alumni Professor of Mechanical Engineering.

Introduction

IN a large-caliber gun system using unslotted single-perforated stick propellants, the interior ballistic performance

could be influenced significantly by the effects of erosive burning. In order to analyze and predict the performance of large-caliber gun systems using stick propellants, the erosive-burning characteristics of the propellants must be determined. In the past, erosive burning of various solid propellants was studied extensively under different crossflow situations.[1] However, prior to the present study, no suitable theoretical model was specifically developed to simulate erosive-burning processes occurring inside the stick perforation of NOSOL-363 or low vulnerability ammunition (LOVA) propellants. This is due to the fact that NOSOL-363 and LOVA propellants have a distended flame structure and introduce stronger interaction of combustion and turbulence.[2] This interaction cannot be modeled properly by previous theoretical approaches. It is apparent that a more sophisticated theoretical model is needed to characterize these erosive-burning processes. The objectives of this study are 1) to formulate a theoretical model to describe erosive-burning phenomena, with special emphasis on turbulence-combustion interaction; 2) to solve the theoretical model numerically; 3) to validate the theoretical model by experimental data; and 4) to study the erosive-burning characteristics of stick propellants.

Theoretical Modeling

The physical model considered in this study consists of two different regions: gas phase and solid phase. The gas-phase region is occupied by an axisymmetric turbulent reacting flow inside the perforation of an unslotted stick propellant (see Fig. 1). The solid-phase region is a NOSOL-363 propellant with an initial geometry of a thick-walled cylindrical tube with uniform inner and outer diameters. To study the erosive effect, only the internal perforation surface is allowed to burn.

Two basic assumptions are made in formulating the model. First, the mean flow is treated as quasisteady, since the flow residence time is much shorter than the characteristic times associated with conduction in the solid propellant and surface regression. This assumption was generally made in earlier erosive-burning studies. Second, it is assumed that the heat flux in the direction normal to the propellant surface is dominant because of strong heat feedback from the flame zone. Thus, the axial heat conduction is considered to be negligible.

As pointed out by Fifer,[2] the combustion mechanism of nitramine-based LOVA propellants is very similar to that of nitrate ester homogeneous propellants such as nitrocellulose/nitroglycerin (NC/NG) double-base propellants. Following the description of flame structure provided by Wu et al.[3] and Kuo et al.,[4] the reaction regions for gas/solid interface and gas phase consist of five different zones, i.e., preheat, foam, fizz, dark, and luminous flame.

Under the conditions of zero or low crossflow velocities, Kubota[5] found significant flame standoff distances for both double-base and nitramine propellants. Under strong crossflow conditions, the flame could be highly distorted, or even form pieces of flamelets; hence, the location of the heat-release zone produced by the reaction of pyrolyzed ingredients could be quite different from the location of pyrolysis. Finite-rate chemical reaction kinetics and the interaction of turbulence and combustion must therefore be considered in the erosive-burning model in order to simulate combustion processes inside the perforation of a stick propellant made of nitrate ester homogeneous propellants.

In modeling chemical reactions, the following reaction mechanism was adopted from Wu et al.[3] For surface pyrolysis of stick propellant, we have

$$\text{stick propellant} \rightarrow \nu_O O + \nu_F F + \nu_{DR1} DR1 \tag{1}$$

where O represents the oxidizer-rich gases (such as NO_2) pyrolyzed from the surface, F represents the fuel-rich species (such as CH_2O), and the remaining species are designated as the first group of delayed reaction species $DR1$. Three chemical reactions considered to take place in the gas phase are

$$\nu_F F + \nu_O O \rightarrow \nu_{DR2} DR2 \tag{2a}$$

$$\nu_{DR1} DR1 \rightarrow \nu_{P1} P \tag{2b}$$

$$\nu_{DR2} DR2 \rightarrow \nu_{P2} P \tag{2c}$$

where $DR2$ represents the intermediate product generated from the reaction in the fizz zone. After a delay in the dark zone, the $DR2$ reacts in the luminous flame zone to generate the final product. Group 1 of delayed reaction species also forms the final product in the final flame.

The stoichiometric coefficients ν_i in Eqs. (2a-2c) are determined from the mass balance of the above four reactions. The heat of formation of these representative groups of species is obtained from the chemical equilibrium code (CEC76).[6] Detailed procedures are described in Refs. 3 and 4.

It is well-known that one major aspect in modeling turbulent reacting flow lies in the handling of the time-averaged chemical production term which is complicated by the interaction of turbulence and combustion. The effect of inevitable fluctuations of flow properties in this source term is difficult to model. One logical way to circumvent this difficulty is to adopt a two-variable joint probability density function (pdf) to obtain statistically averaged physical properties.[7]

The approach used in modeling the chemical production term is similar to that of Janicka and Kollmann[8] in their studies of turbulent H_2-air diffusion flames. The present approach differs in the selection of independent variables. Janicka and Kollmann used the mixture fraction with a single reactedness; the present approach adopts two reactednesses due to the fact that in premixed flames it is impossible to use mixture fraction as one of the independent variables. One specific feature of the present approach is similar to that of Bray and Moss,[9] who also used a joint pdf with two reactednesses as independent variables. In their studies, two consecutive reactions were used to simulate hydrocarbon-air combustion, whereas a set of competitive and consecutive reactions are considered in the present study.

The two independent variables chosen for the pdf are reactednesses of reactions, Eqs. (2a) and (2b). They are defined as

$$R_A \equiv \frac{Y_F - Y_{F,u}}{Y_{F,b} - Y_{F,u}} \tag{3a}$$

$$R_B \equiv \frac{Y_{DR1} - Y_{DR1,u}}{Y_{DR1,b} - Y_{DR1,u}} \tag{3b}$$

The transport equations for mean reactednesses and mean-square fluctuations of reactednesses[8] are given as

$$\bar{\rho}\,\tilde{u}\frac{\partial \tilde{R}}{\partial x} + \bar{\rho}\,\tilde{v}\frac{\partial \tilde{R}}{\partial r} = \frac{1}{r}\frac{\partial}{\partial r}\left[r\left(\frac{\mu}{Sc}\right)_{eff}\frac{\partial \tilde{R}}{\partial r}\right] + \dot{\bar{\omega}}_R \tag{4}$$

$$\bar{\rho}\tilde{u}\frac{\partial \widetilde{R''^2}}{\partial r} + \bar{\rho}\tilde{v}\frac{\partial \widetilde{R''^2}}{\partial r} = \frac{1}{r}\frac{\partial}{\partial r}\left[r\left(\frac{\mu}{Sc}\right)_{eff}\frac{\partial \widetilde{R''^2}}{\partial r}\right]$$

$$+ C_{R_1}\mu_t\left(\frac{\partial \tilde{R}}{\partial r}\right)^2 - C_{R_2}\bar{\rho}\frac{\epsilon}{k}\widetilde{R''^2} + \overline{2R''\dot{\omega}} \tag{5}$$

where R can be either R_A or R_B.

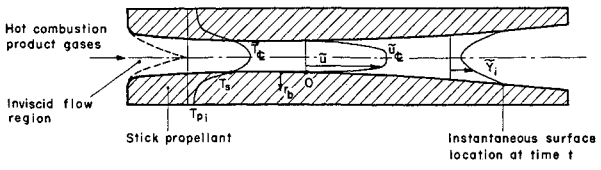

Fig. 1 Flow and temperature fields inside an unslotted single-perforated stick propellant.

In general, there are two approaches to determine the relationship between the pdf and the two selected variables. One approach is to solve the equation of evolution of the pdf. The modeling of the pdf evolution equation was proposed by Dopazo,[10] Pope,[11] and O'Brien,[12] and applied to turbulent diffusion flame by Janicka et al.[13] This approach was not adopted in the present study because of the extraordinary numerical effort required to solve the evolution equation. The second approach, to assume a functional relationship between the pdf and selected variables, has been used extensively in calculation of different turbulent diffusion or premixed flames.[8,9] In this study, a simple beta functional form was chosen to relate the pdf to the two reactedness and their variants. The beta pdf is defined as

$$\mathcal{P}(R) = \frac{R^{\alpha-1}(1-R)^{\beta-1}}{\int_0^1 R^{\alpha-1}(1-R)^{\beta-1}\,dR} \tag{6}$$

where

$$\alpha = \tilde{R}\left[\frac{\tilde{R}(1-\tilde{R})}{\widetilde{R''^2}} - 1\right] \tag{7}$$

$$\beta = (1-\tilde{R})\left[\frac{\tilde{R}(1-\tilde{R})}{\widetilde{R''^2}} - 1\right] \tag{8}$$

Under the assumption that R_A and R_B are not correlated, the joint probability function $\mathcal{P}_J(R_A, R_B)$ can be expressed as

$$\mathcal{P}_J(R_A, R_B) = \mathcal{P}(R_A)\cdot\mathcal{P}(R_B) \tag{9}$$

By using pdf, mean chemical production terms in Eqs. (4) and (5) can be expressed as

$$\overline{\dot{\omega}_R} = \int_0^1\int_0^1 \dot{\omega}_R\,\mathcal{P}_J(R_A, R_B)\,dR_A\,dR_B \tag{10}$$

$$\overline{R''\dot{\omega}_R} = \int_0^1\int_0^1 (R-\tilde{R})\dot{\omega}_R\,\mathcal{P}_J(R_A, R_B)\,dR_A\,dR_B \tag{11}$$

The instantaneous chemical production term[3] is given by

$$\dot{\omega}_R = -A_F \exp(-E_{a,F}/R_uT)\rho^2 Y_F Y_O/W_O/(Y_{F,b} - Y_{F,u}) \quad \text{for } R = R_A \tag{12a}$$

$$\dot{\omega}_R = -A_{DR1} \exp(-E_{a,DR1}/R_uT)\rho^2 Y_{DR1}^2/W_{DR1}/(Y_{DR1,b} - Y_{DR1,u}), \quad \text{for } R = R_B \tag{12b}$$

For premixed flames, in circumstances in which all species are assumed to have the same coefficient of diffusion transport, the carbon element mass fraction Z_c and the Schvab-Zeldovich variable ξ can be regraded as constants, i.e.,

$$Z_c = \sum(\mu_{cj})Y_j = \text{constant} \tag{13}$$

$$\xi = Y_O - \left(\frac{\nu_O W_O}{\nu_F W_F}\right)Y_F = \text{constant} \tag{14}$$

The sum of the mass fractions for all species is equal to one, i.e.,

$$\sum_i Y_i = 1 \tag{15}$$

The mass fractions of all five species can be solved from five algebraic equations [including Eqs. (3a), (3b), (13), (14), and (15), after $\tilde{R}_A$ and $\tilde{R}_B$ are solved from Eqs. (4) and (5).

The turbulent flow inside the center perforation of the stick propellant can be described by the following set of conservation equations for mass, momentum, total enthalpy, transport equation of turbulent kinetic energy, and transport equation of turbulent dissipation rate, as well as the equation of state in the Favre-averaged form. These equations were derived with the following assumptions: 1) Favre-averaged flow properties are quasisteady; 2) boundary layer is axisymmetric; 3) body force and gas-phase radiation heat transfer are negligible; 4) Soret or Dufour effects are small; and 5) Fick's law of mass diffusion is valid.

$$\frac{\partial}{\partial x}(r\,\bar{\rho}\,\tilde{u}) + \frac{\partial}{\partial r}(r\,\bar{\rho}\,\tilde{v}) = 0 \tag{16}$$

$$\bar{\rho}\,\tilde{u}\frac{\partial\tilde{u}}{\partial x} + \bar{\rho}\,\tilde{v}\frac{\partial\tilde{u}}{\partial r} = \frac{1}{r}\frac{\partial}{\partial r}\left(r\,\mu_{eff}\frac{\partial\tilde{u}}{\partial r}\right) - \frac{d\bar{p}}{dx} \tag{17}$$

$$\bar{\rho}\,\tilde{u}\frac{\partial\tilde{H}}{\partial x} + \bar{\rho}\,\tilde{v}\frac{\partial\tilde{H}}{\partial r} = \frac{1}{r}\frac{\partial}{\partial r}\left\{r\left[\left(\frac{\mu}{Pr}\right)_{eff}\frac{\partial\tilde{H}}{\partial r} + \left\{\mu_{eff} - \left(\frac{\mu}{Pr}\right)_{eff}\right\}\frac{\partial\tilde{u}^2/2}{\partial r}\right]\right\} \tag{18}$$

$$\bar{\rho}\,\tilde{u}\frac{\partial k}{\partial x} + \bar{\rho}\,\tilde{v}\frac{\partial k}{\partial r} = \frac{1}{r}\frac{\partial}{\partial r}\left[r\left(\mu + \frac{\mu_t}{C_1}\right)\frac{\partial k}{\partial r}\right] + \mu_t\left(\frac{\partial\tilde{u}}{\partial r}\right)^2 - \bar{\rho}\,\epsilon \tag{19}$$

$$\bar{\rho}\,\tilde{u}\frac{\partial\epsilon}{\partial x} + \bar{\rho}\,\tilde{v}\frac{\partial\epsilon}{\partial r} = \frac{1}{r}\frac{\partial}{\partial r}\left[r\left(\mu + \frac{\mu_t}{C_2}\right)\frac{\partial\epsilon}{\partial r}\right] + C_3\mu_t\left(\frac{\partial\tilde{u}}{\partial r}\right)^2\frac{\epsilon}{k} - C_4\bar{\rho}\frac{\epsilon^2}{k} \tag{20}$$

$$\bar{p} = \frac{R\tilde{T}}{[(1/\bar{\rho}) - b]} \tag{21}$$

Turbulent viscosity μ_t is expressed in terms of k and ϵ as

$$\mu_t = c_\mu\bar{\rho}\frac{k^2}{\epsilon} \tag{22}$$

In deriving the above equations, the following relationships were used.

$$-\overline{\rho u''v''} = \mu_t\frac{\partial\tilde{u}}{\partial r}, \qquad -\overline{\rho v''R''} = \frac{\mu_t}{Sc_t}\frac{\partial\tilde{R}}{\partial r}, \qquad -\overline{\rho v''H''} = \frac{\mu_t}{Pr_t}\frac{\partial\tilde{H}}{\partial r} \tag{23}$$

Turbulent constants used in the above governing equations are listed in Table 1.

To determine the instantaneous temperature profile in the stick propellant, as well as the surface-temperature distribution, a transient one-dimensional heat conduction equation is

Table 1 Constants used in turbulence modeling

Constant	Value	Refs.
C_1	1.0	14–16
C_2	1.3	14–16
C_3	1.57	16
C_4	2.0	17
C_μ	0.09	14–16
C_{R_1}	2.7	8
C_{R_2}	1.79	8

considered. This equation[18] is given as

$$\rho_s \frac{\partial(C_s T_s)}{\partial t} = \frac{1}{r}\frac{\partial}{\partial r}\left(r\lambda_s \frac{\partial T_s}{\partial r}\right) + a[(I_r - E_b) + (J_r - E_b)] \quad (24)$$

which takes into account the subsurface radiation absorption for translucent propellants such as NOSOL-363. The determination of the source terms containing both outward and inward radiant fluxes requires solution of the flux-transport equations. Based on a two-flux model,[18] the two transport equations for I_r and J_r can be given as

$$\frac{\mathrm{d}(rI_r)}{\mathrm{d}r} = -(s+a)rI_r + arE_b + J_r + \frac{1}{2}sr(I_r + J_r) \quad (25)$$

$$\frac{\mathrm{d}(rJ_r)}{\mathrm{d}r} = (s+a)rJ_r - arE_b + J_r - \frac{1}{2}sr(I_r + J_r) \quad (26)$$

A set of boundary and initial conditions must be specified to complete the theoretical formulation. At the solid-gas interface, balances of mass and energy fluxes can be written as

$$\rho_s r_b Y_{i,s} = (\bar{\rho}\tilde{v}\tilde{Y}_i)_g - \left(\rho D \frac{\partial \tilde{Y}_i}{\partial r}\right)_g \quad (27)$$

$$-\lambda \left.\frac{\partial T_s}{\partial r}\right|_s = (\dot{q}''_{\mathrm{rad}})_{\mathrm{net}} - \lambda_g \left.\frac{\partial \tilde{T}}{\partial r}\right|_g$$

$$+ \rho_s r_b[(C_s - C_p)\cdot(T_s - T_{s,\mathrm{ref}}) + Q_{s,\mathrm{ref}})] \quad (28)$$

where $Q_{s,\mathrm{ref}}$ is defined as the net surface heat release at reference temperature $T_{s,\mathrm{ref}}$; $(\dot{q}''_{\mathrm{rad}})_{\mathrm{net}}$ is the net radiation flux on the interface, and is related to I_r and J_r by the following equation.

$$(\dot{q}''_{\mathrm{rad}})_{\mathrm{net}} = I_r\Big|_{r=r_i^-} + \epsilon_s J_r\Big|_{r=r_i^+} - \epsilon_s \sigma T_{ps}^4 \quad (29)$$

Other boundary conditions at the solid-gas interface are

$$\tilde{u} = 0, \qquad \tilde{v} = \rho_s r_b/\bar{\rho}_g, \qquad \widetilde{R''^2_A} = \widetilde{R''^2_B} = 0 \quad (30)$$

which represent nonslip condition, mass continuity, and zero fluctuation of reactednesses, respectively. The boundary conditions for the k and ϵ equations at the near-wall region are identical to those of Arora et al.[19]

When the flow inside the perforation of the stick propellant is not fully developed, flow properties are considered to be either continuous or constant at the edge of the boundary layer, i.e.,

$$\tilde{u} = u_{\ell}, \qquad \tilde{T} = T_{\ell}, \qquad \frac{\partial k}{\partial r} = \frac{\partial \epsilon}{\partial r} = 0 \quad (31)$$

$$\tilde{R}_A = 1, \qquad \tilde{R}_B = 1, \qquad \frac{\partial \widetilde{R''^2_A}}{\partial r} = \frac{\partial \widetilde{R''^2_B}}{\partial r} = 0 \quad (32)$$

When the flow is fully developed, the symmetric conditions are used at the axis, i.e.,

$$\frac{\partial \tilde{u}}{\partial r} = \frac{\partial \tilde{T}}{\partial r} = \frac{\partial k}{\partial r} = \frac{\partial \epsilon}{\partial r} = \frac{\partial \tilde{R}_A}{\partial r} = \frac{\partial \tilde{R}_B}{\partial r}$$
$$= \frac{\partial \widetilde{R''^2_A}}{\partial r} = \frac{\partial \widetilde{R''^2_B}}{\partial r} = \frac{\partial \tilde{H}}{\partial r} = 0 \quad (33)$$

The initial condition for the solid-phase heat-conduction equation is

$$T_p = T_{pi}, \qquad \text{at } t = 0 \quad (34)$$

where T_{pi} is the initial temperature of the propellant.

Boundary conditions for Eq. (24) and the radiative heat-flux equation at the gas-solid interface are

$$T_p|_{r=r_i} = \tilde{T}_g|_{r=r_i} \quad (35)$$

$$I_r = (1 - \Re_p)\sigma \tilde{T}^4_{g_{\mathrm{eff}}} - \epsilon_s \sigma T_{ps}^4 + \Re_p J_r \quad (36)$$

and at the outer radius are

$$T_p|_{r=r_o} = T_{pi} \quad (37)$$

$$J_r = (1 - \Re_p)\sigma T_w^4 - \epsilon_s \sigma T_{pi}^4 \quad (38)$$

The initial k and ϵ profiles were calculated from the following equations.[20]

$$k = \frac{u_*^2}{\sqrt{c_\mu}} \cos^2\left(\frac{1}{2}\pi y/\delta\right) \quad (39)$$

$$\epsilon = \begin{cases} \dfrac{u_*^3}{ky}\cos^3\left(\dfrac{1}{2}\pi y/\delta\right) & y \le 0.09\,\delta/k \\ \dfrac{u_*^3}{0.09\delta}\cos^3\left(\dfrac{1}{2}\pi y/\delta\right) & y > 0.09\,\delta/k \end{cases} \quad (40)$$

The set of gas-phase simultaneous partial differential equations was solved by the implicit, finite-difference method of Patankar and Spalding.[21] Using a central-difference technique, the transient heat-conduction equation and radiation heat-flux equations were solved for the solid phase to obtain the temperature distributions in the stick propellant as a function of time. Detailed finite-difference equations and numerical procedures for both regions can be found in Refs. 22 and 23.

Experimental Work

In this study, a test rig using a center-perforated cylindrical propellant grain with large web thickness (~ 1.0 cm) was designed and constructed to observe erosive-burning phenomena and to obtain a data base for model validation. Instantaneous locations of the internal burning surface of a cylindrical stick-propellant grain were determined by real-time x-ray radiography, which consists of a constant potential continuous-wave x-ray system, an image intensifier, a Spin Physics high-speed digitized movie system, and a digital image-processing system. Detailed descriptions of the test chamber design, real-time x-ray radiography system, and data-acquisition system can be found in Ref. 24.

Discussion of Results

In order to perform the numerical simulation of erosive-burning processes inside the internal perforation of a NOSOL-363 stick propellant, a set of physical and chemical properties of NOSOL-363 must be supplied as input to the computer code. The chemical ingredients of the NOSOL-363 stick propellant and their molecular weights, mass fractions, and heats of formation are given in Table 2. The other properties used in the calculation are given in Table 3. Sources of references for some of the properties are also given in Table 3.

Figure 2 shows the comparison between the calculated radius and experimental data obtained under erosive-burning conditions.[24] Theoretical predictions compare well with measured data at various times. Time variation of erosive-burning rates along the propellant grain is shown in Fig. 3. The burning rate apparently decreases as time increases, due to the fact that pressure and mass flux flowing over the burning surface decrease with respect to time (see Fig. 4). In the early time period ($t < 0.37$ s), the burning rates at downstream locations are higher than those at upstream locations because of increased mass flow rate in the downstream direction. As time passes, the cross-flow velocity drops as the port area increases, and the effect of pressure becomes more important. This causes the site of maximum burning to move in the upstream direction.

Table 2 Chemical ingredients of the NOSOL-363 propellant and their molecular weights, mass fractions, and heats of formation

Ingredient name	Chemical composition	Molecular weight, kg/kmole	Mass fraction, %	Δh_f^o, kJ/kg
NC 1265 (nitrocellulose)	$C_6H_{7.55}O_5(NO_2)_{2.45}$	272.25	45.75	−2583.8
METRZO (metriol trinitrate)	$C_5H_9O_3(NO_2)_3$	255	40.92	−1737.6
TEGDN (triethylene glycol dinitrate)	$C_6H_{12}O_4(NO_2)_2$	240	10.07	−2261.5
DNPA (di-normal propyl adipate)	$C_{12}H_{22}O_4$	232	0.98	−3736.5
EC (ethyl centralite)	$C_{17}H_{20}ON_2$	268	1.05	−391.5
KS (potassium sulfate)	K_2SO_4	174.1	0.97	−8231.7

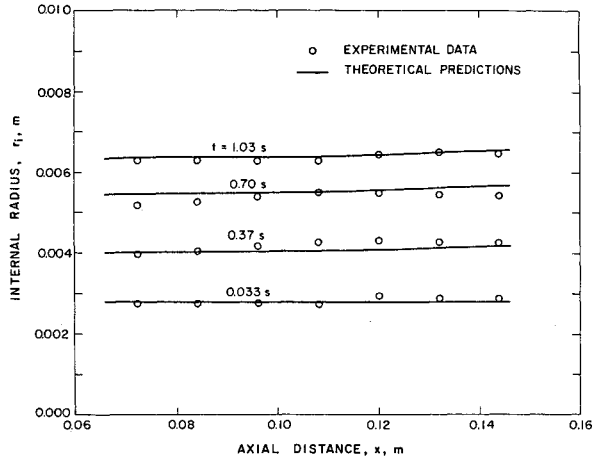

Fig. 2 Comparison between calculated internal radius and experimental data obtained from erosive-burning test using a thick-walled NOSOL-363 stick-propellant grain (Test No. 24).

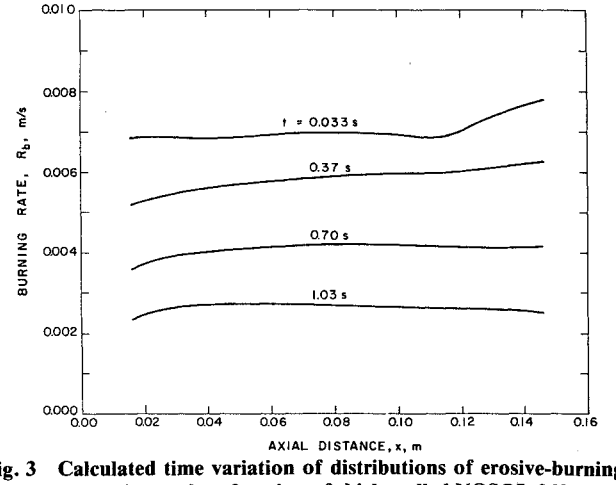

Fig. 3 Calculated time variation of distributions of erosive-burning rates along the internal perforation of thick-walled NOSOL-363 stick-propellant grain.

Figure 5 shows the calculated velocity profiles at three axial positions. The centerline velocity is increasing with x due to mass addition and growth of boundary-layer thickness along the axial direction. Because of the higher mass injection rate from the burning propellant surface, the velocity profile becomes fuller at downstream locations. These phenomena were also reported by Trainean et al.[25] in experimental data obtained in a cold-flow test of a nozzleless rocket motor.

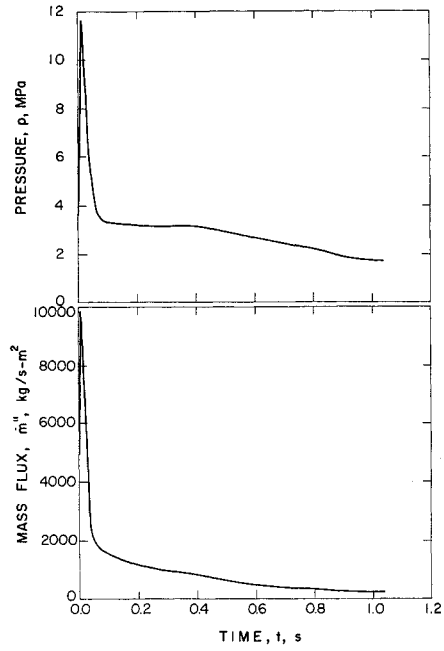

Fig. 4 Time variations of pressure and mass flux at $x = 1.6$ cm.

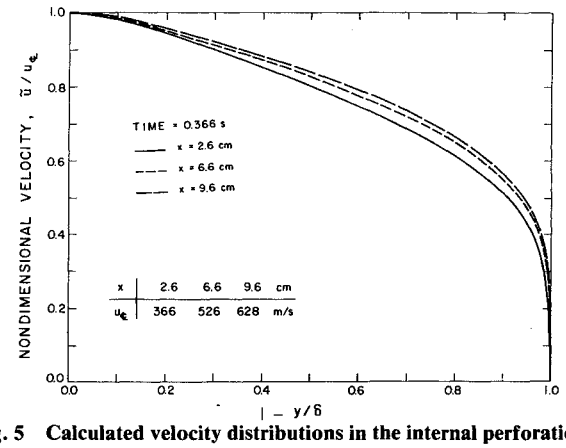

Fig. 5 Calculated velocity distributions in the internal perforation of a thick-walled NOSOL-363 stick-propellant grain.

The distributions of turbulence kinetic energy at different axial positions are shown in Fig. 6. As x increases, the magnitude of turbulence kinetic energy increases, indicating the enhanced turbulent heat- and mass-transfer rates at downstream locations. The enhanced turbulent heat-transfer rate at a downstream location causes more energy to be transferred from the gas phase to the propellant surface, resulting in higher burning surface temperature and burning rate. This trend of increased turbulence energy was also reported by Yamada et al.[26] and Trainean et al.[24]

Figure 7 shows a set of distributions of mass fractions of fuel, oxidizer, and delayed reaction species of group 1 (*DR* 1) at three different axial locations. The concentration profiles of these species are quite steep near the propellant surface. This implies that a certain portion of the chemical reactions occur very near the propellant surface. From the overall mass-fraction distributions, it is also noted that the chemical reactions away from the propellant surface are not insignificant. The interaction of turbulence with chemical reactions is important throughout most portions of the reacting boundary layer.

In order to examine the effect of various important thermophysical and thermochemical properties on the erosive-burning rate, a parametric study was conducted with the numerical

Table 3 Thermochemical and thermophysical properties used in the numerical calculation

Property	Value	Ref.	Property	Value	Ref.
A_{DR1}	$= 1.7 \times 10^{10}$ m³/kmole-s	5	ν_{p1}	= 1.677 kmole	
A_F	$= 1.0 \times 10^{7}$ m³/kmole-s	5	ν_{p2}	= 3.769 kmole	
W_{DR1}	= 24.94 kg/kmole		C_{p0}	= 1.19 kJ/kg-K	
W_{DR2}	= 30.44 kg/kmole		C_{pF}	= 2.32 kJ/kg-K	
W_F	= 30.03 kg/kmole		C_{pDR1}	= 1.73 kJ/kg-K	
W_O	= 46.01 kg/kmole		C_{pDR2}	= 1.44 kJ/kg-K	
W_P	= 22.83 kg/kmole		C_{pp}	= 1.90 kJ/kg-K	
$Y_{DR1,s}$	= 0.3083		γ	= 1.24	
$Y_{DR2,s}$	= 0.0		Pr	$= \gamma/(1.77\,\gamma - 0.45)$	28
$Y_{F,s}$	= 0.2411		Pr_t	= 0.9	29
$Y_{O,s}$	= 0.4506		μ_g	$= 8.7 \times 10^{-8} \sqrt{W_g T_g}\ 0.65$	28
$E_{a,DR1}$	= 209 kJ/mole	5	σ	$= 5.669 \times 10^{-8}$ W/m²-K⁴	
$E_{a,F}$	= 33.5 kJ/mole	5	ρ_s	= 1530 kg/m³	
$\Delta h^o_{f,DR1}$	= −3628 kJ/kg		C_s	= 1675 J/kg-K	
$\Delta h^o_{f,DR2}$	= −7381 kJ/kg		α_s	$= 1.70 \times 10^{-7}$ m²/s	
$\Delta h^o_{f,F}$	= −3862 kJ/kg		$\Re_p$	= 0.1	23
$\Delta h^o_{f,O}$	= 736.5 kJ/kg		a	= 200 1/m	23
$\Delta h^o_{f,P}$	= −5740 kJ/kg		ϵ_s	= 0.9	23
ν_{DR1}	= 1.536 kmole		$E_{a,s}$	= 34.0 kJ/mole, $p < 2.17$ MPa	27
ν_{DR2}	= 2.827 kmole			= 62.0 kJ/mole, $p > 2.17$ MPa	27
ν_F	= 1 kmole		A_s	= 0.79 m/s, $p < 2.17$ MPa	27
ν_O	= 1.2 kmole			= 92.4 m/s, $p > 2.17$ MPa	27

Table 4 Parametric study of the effect of various important thermophysical and thermochemical properties on the calculated erosive-burning rate

Property	Effect on the erosive-burning rate, %[a]
A_{DR1}	+ 0.25
A_F	+ 1.13
A_s	+ 7.75
α_s	− 4.46
ϵ_s	+ 0.28
$E_{a,DR1}$	− 0.86
$E_{a,F}$	− 1.70
$E_{a,s}$	− 20.13
$\Re_p$	− 0.005
a	+ 0.003

[a]The effect of a property is evaluated by the percentage change in the burning rate at $t = 0.013$ s and $x = 0.126$ m, as the value of the property is increased by 10% from that listed in Table 3.

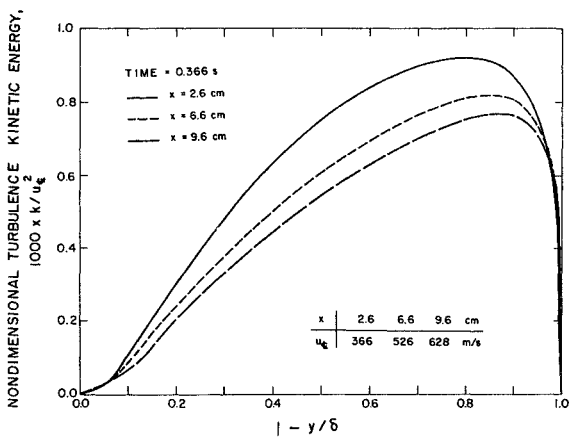

Fig. 6 Calculated turbulence kinetic energy distributions in the internal perforation of a thick-walled NOSOL-363 stick-propellant grain.

code developed in this research work. The results of the parametric study presented in Table 4 show that the A_s and $E_{a,s}$ used in the pyrolysis law to evaluate the burning rate have the strongest effect on the erosive-burning rate, indicating that the erosive-burning phenomenon is influenced significantly by the surface pyrolysis process. For the gas-phase reactions, the A_F and $E_{a,F}$ have a greater effect on the erosive-burning rate than the A_{DR1} and $E_{a,F}$, since the oxidation of the fuel is the major heat-release mechanism in the gas-phase region. It is interest-

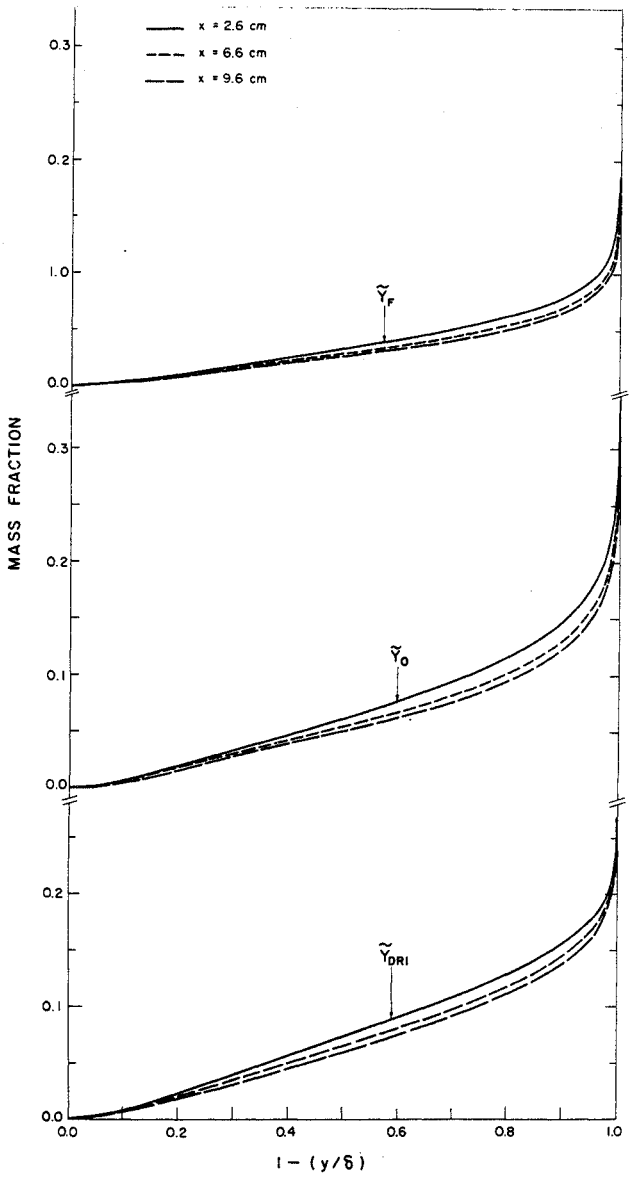

Fig. 7 Calculated distributions of mass fractions of oxidizer, fuel, and *DR*1 in the internal perforation of a thick-walled NOSOL-363 stick-propellant grain.

ing to note that the various radiative properties of the propellant have different degrees of effect on the erosive-burning rate, with the surface absorption coefficient exerting the greatest effect. This is caused by the fact that the radiative energy absorbed by the burning surface increases as the value of the absorption coefficient increases, which then increases the burning surface temperature to enhance the erosive-burning rate.

Besides the properties listed in Table 4, the effect of the initial profiles of k and ϵ at $x = 0$ on the erosive-burning rate is also studied. Similar to the parametric study for other properties, this effect is evaluated by the percentage change in the erosive-burning rate at $t = 0.013$ s as the magnitudes of k and ϵ at $x = 0$ and different radial locations were increased by a factor of 10%. From this study, it was found that the initial profiles of k and ϵ do not have a significant effect on the erosive-burning rate calculated from the numerical code, since the solutions for the parabolic type of governing equations are known for being insensitive to the initial conditions. When the magnitudes of k at $x = 0$ is increased by 10%, the erosive-burning rate is increased by 1.9, 1.83, and 0.22% at $x = 0.016$, 0.026, and 0.036 m, respectively. The effect of the initial profile of ϵ is even smaller than that of k.

Summary and Conclusions

1) A comprehensive theoretical model was formulated to simulate erosive-burning processes occurring inside a center perforation of a stick propellant.

2) The comprehensive erosive-burning model was solved numerically and validated by experimental data. The calculated time variation of internal radius distribution along the grain agrees well with measured distributions.

3) Chemical reactions occur throughout the turbulent reacting boundary layer of a stick propellant. Therefore, interaction of turbulence and combustion is important in the entire boundary layer.

4) Burning rates along the center perforation of a stick propellant depend strongly upon local pressures and crossflow velocities. When both pressure and crossflow velocity decreases, the burning rate decreases.

5) From numerical solutions, the erosive burning is found to be caused by the enhanced heat feedback from the gas phase to solid propellant resulting from the combined effect of increased turbulence kinetic energy and turbulent heat-transfer rate.

Acknowledgments

This research represents a part of the results obtained under Contract DAAK29-83-K-0081, sponsored by Engineering Sciences Division, Army Research Office, Research Triangle Park, NC, under the management of David M. Mann. The authors would also like to acknowledge the encouragement and support of David Downs of ARDEC-Dover and F. Robbins of Ballistic Research Laboratory, Aberdeen Proving Ground, MD.

References

[1]Razdan, M. K., and Kuo, K. K., "Fundamentals of Solid-Propellant Combustion," edited by K. K. Kuo and M. Summerfield, Vol. 90, *Progress in Astronautics and Aeronautics,* AIAA, New York, 1984, Chap. 10.

[2]Fifer, R. A., "Fundamentals of Solid-Propellant Combustion," edited by K. K. Kuo and M. Summerfield, *Progress in Astronautics and Aeronautics,* Vol. 90, AIAA, New York, 1984, Chap. 4.

[3]Wu, X., Kumar, M., and Kuo, K. K., "A Comprehensive Erosive-Burning Model for Double-Based Propellants in Strong Turbulent Shear Flow," *Combustion and Flame,* Vol. 53, Nov. 1983, pp. 49–63.

[4]Kuo, K. K., Hsieh, K. C., and Athavale, M., "Modeling of Combustion Processes of Stick Propellants via Combined Eulerian-Lagrangian Approach," *Proceedings of the Eighth International Symposium on Ballistics,* The American Defense Preparedness Association, Wilmington, MA, 1984, pp. 155–168.

[5]Kubota, N., "Fundamentals of Solid-Propellant Combustion," *Progress in Astronautics and Aeronautics,* edited by K. K. Kuo and M. Sumerfield, Vol. 90, AIAA, New York, 1984, Chap. 1.

[6]Gordon, S., and McBride, B. J., "Computer Program for Calculation of Complex Chemical Equilibrium Compositions, Rocket Performance, Incident and Reflected Shocks, and Chapman-Jouguet Detonations," NASA SP-273 Interim Revision N78-17724, March 1976.

[7]Libby, P. A., and Williams, F. A. (eds.), *Turbulent Reacting Flows,* Springer-Verlag, Berlin-Heidelberg, New York, 1980.

[8]Janicka, J., and Kollmann, W., "A Two-Variables Formalism for the Treatment of Chemical Reactions in Turbulent H_2-Air Diffusion Flames," *17th International Symposium on Combustion,* The Combustion Institute, Pittsburgh, PA, 1979, pp. 421-430.

[9]Bray, K. N. C., and Moss, J. B., "A Closure Model for the Turbulent Premixed Flame with Sequential Chemistry," *Combustion and Flame,* Vol. 30, No. 2, Aug. 1978, pp. 125–131.

[10]Dopazo, C., "An Approach to Autoignition of a Turbulent Mixture," *Acta Astronautica,* Vol. 1, Sept.–Oct. 1974, p. 1239.

[11]Pope, S. B., "The Probability Approach to the Modeling of Turbulent Reacting Flows," *Combustion and Flame,* Vol. 27, Dec. 1976, pp. 299–312.

[12]O'Brien, E. E., *Turbulent Reacting Flows,* edited by P. A. Libby, and F. A. Williams, Springer-Verlag, Berlin-Heidelberg, New York, 1980, Chap. 4.

[13]Janicka, J. S., Kolba, W., and Kollmann, W., *Proceedings of the 1978 Heat Transfer and Fluid Mechanics Institute,* edited by C. T. Crowe, and W. L. Grosshandler, Stanford Univ. Press, San Francisco, CA, 1978, p. 296.

[14]Launder, B. E., and Spalding, D. B. *Mathematical Models of Turbulence,* Academic, Orlando, 1972.

[15]Gosman, A. D., Lockwood, F. C., and Syed, S. A., "Prediction of a Horizontal Free Turbulent Diffusion Flame," *16th International Symposium on Combustion,* The Combustion Institute, Pittsburgh, PA, 1976, pp. 1543–1555.

[16]Lockwood, F. C., and Naguib, A. S., "The Prediction of the Fluctuations in the Properties of Free, Round-Jet, Turbulent, Diffusion Flames," *Combustion and Flame,* Vol. 24, No. 1, Feb. 1975, pp. 109–124.

[17]Elghobashi, S. E., and Pun, W. M., "A Theoretical and Experimental Study of Turbulent Diffusion Flames in Cylindrical Furnaces," *15th International Symposium on Combustion,* The Combustion Institute, Pittsburgh, PA, 1974, pp. 1353–1365.

[18]Gosman, A. D., and Lockwood, F. C., "Incorporation of a Flux Model for Radiation into a Finite-Difference Procedure for Furnace Calculation," *14th International Symposium on Combustion,* The Combustion Institute, Pittsburgh, PA, 1973, pp. 661–671.

[19]Arora, R., Kuo, K. K., and Razdan, M. K., "Near-Wall Treatment for Turbulent Boundary-Layer Computations," *AIAA Journal,* Vol. 20, Nov. 1982, pp. 1481–1482.

[20]Chamber, T. L., and Wilcox, D. C., "Critical Examination of Two-Equation Turbulence Closure Models for Boundary Layers," *AIAA Journal,* Vol. 15, June 1977, pp. 821–828.

[21]Patankar, S. V., and Spalding, D. B., *Heat and Mass Transfer in Boundary Layers,* Inter-Text Books, London, 1970.

[22]Razdan, M. K., and Kuo, K. K., "Measurements and Model Validation for Composite Propellants Burning under Crossflow of Gases,"*AIAA Journal,* Vol. 18, June 1980, pp. 669–677.

[23]Hsieh, K. C., "Combustion of Unslotted Stick-Propellant Bundles in Simulated Gun Environment," Ph.D. Thesis, The Pennsylvania State University, University Park, PA, May 1987.

[24]Hsieh, W. H., Char, J. M., Hsieh, K. C., and Kuo, K. K., "Modeling and Measurement of Erosive Burning of Stick Propellants," AIAA Paper 86-1451, June 1986.

[25]Trainean, J. C., Hervat, P., and Kuentzmann, P., "Cold-Flow Simulation of a Two-Dimensional Nozzleless Solid Rocket Motor," AIAA Paper 86-1467, June 1986.

[26]Yamada, K., Goto, M., and Ishikawa, N., "Simulative Study on the Erosive Burning of Solid Rocket Motors," *AIAA Journal,* Vol. 14, Sept. 1976, pp. 1170–1177.

[27]Hsieh, W. H., "Study of Strand and Erosive Burning of NOSOL-363 Stick Propellants," Ph.D. Thesis, The Pennsylvania State University, University Park, PA, June 1987.

[28]Peretz, A., Kuo, K. K., Caveny, L. H., and Summerfield, M., "Starting Transient of Solid Propellant Rocket Motors with High Internal Gas Velocities," *AIAA Journal,* Vol. 11, Nov. 1973, pp. 1719–1727.

[29]Kays, W. M., "Heat Transfer to the Transpired Turbulent Boundary Layer," *International Journal of Heat and Mass Transfer,* Vol. 15, May 1972, pp. 1023–1044.